A WIRELESS STRUCTURAL HEALTH MONITORING SYSTEM FOR DAMAGE DETECTION IN CONCRETE STRUCTURES BASED ON AN ELECTROMECHANICAL IMPEDANCE-TYPE APPROACH

C. Providakis, S. Tsistrakis, M. Voutetaki, J. Tsompanakis, M. Stavroulaki, J. Agadakos, E. Kampianakis, and G. Pentes

Laboratory of Applied Mechanics, School of Architecture,
Technical University of Crete, GR-73100 Chania, Greece
*Email: cpprov@mred.tuc.gr

ABSTRACT

The present experimental work further investigate and evaluate an innovative monitoring system for various structural health monitoring applications based on an electromechanical impedance (or admittance)-type approach. The system evaluates the variations in the output voltage of piezoelectric transducers and does not compute the impedance (or admittance) itself. The proposed system is a low cost, portable, and wireless measuring system which could efficiently replace commercial instruments in concrete and steel-concrete composite bridge structures. The damage detection is achieved by simply comparing changes in root mean square voltage from response signals produced on the surface of piezoelectric transducers, such as lead zirconate titanate (PZT) patches bonded to the structure. Those changes occur when damage alters the mechanical impedance of the examined concrete structure and when propagating guided waves encounter structural damage. Experimental models of damages occurring in conventional unreinforced and steel-reinforced concrete beams are investigated. Results illustrate that the proposed integrated technique is an efficient approach for damage identification and early detection.

1. INTRODUCTION

The need for real-time, in-situ structural health monitoring (SHM) and damage detection techniques for concrete structures has leaded to develop various successful experimental approaches dedicated to prevent catastrophic failures and to reduce the cost of maintenance and inspecting tasks. One of the most promising experimental techniques is the so called electromechanical impedance (EMI) or its inverse admittance (EMA) approach [1-3]; which uses electromechanical impedance (admittance) spectrum signatures acquired across the electrodes of piezoelectric patches surface bonded or embedded inside the body of concrete structural components. This approach is based on the direct relation existed between the PZT impedance and structural mechanical impedance which, in turn, is affected by the presence of damage.

During the initial years of EMI development, the research efforts mainly focused on exploring the possible application of EMI technique on various mechanical and structural systems using commercialized equipments, such as the Agilent 4294A or the HP 4192A impedance analyzers, which can cost as much as 40,000 US dollars. Those equipments were commonly used to measure the two desired PZT impedance (or its inverse admittance) parameters: the conductance, which is the real part of impedance, and the susceptance, which is the imaginary part of impedance, for each measurement. However, due to the high cost, such equipment may not always be available to be used for the impedance based structural health monitoring process. To address the issues of prohibitive cost and portability, a new PZT active sensing monitoring system has been developed in the present work using an approach which basically has the benefits of hardware simplicity but not limited by the data acquisition (DAQ) device sampling rate which is basically required to replace the high cost commercial impedance analyzers [4-6].

The objective of this paper is to further evaluate a new structural health monitoring system developed by the present authors in [7-8] that uses lea-zirconate-titanate patches (PZT) as sensors and actuators, to detect damage in a concrete structure. This innovative monitoring system includes a wireless telemetry system for measurements storing and retrieving purposes. The system measures the spectrum variations in the peak output voltage response signal, generated across the poles of PZT patches bonded on the surface of the

investigated concrete structures. These variations are directly related to the variations of the electromechanical impedance (admittance) spectrum signatures and behave analogously with them in the presence of damage [9-10]. This idea significantly simplifies the methodology and in connection with the use of a new damage index based on the relation existed between certain probability confidence ellipses to confidence circles of equivalent probability which in other words will represent the variation of the covariance matrix for 2D normally distributed spectrum measurement data, according to a chosen confidence value.

The proposed methodology is effectively applied to the damage detection of concrete beam specimens proving that might be considered as an alternative to conventional structural health monitoring techniques.

2. ELECTRO-MECHANICAL IMPEDANCE (EMI) METHOD

The EMI technique uses piezoelectric materials, such as Lead Zirconate Titanate (PZT), which exhibits the characteristic feature to generate surface charge in response to an applied mechanical stress and conversely, undergo mechanical deformation in response to an applied electric field.

Consider a structural component with a PZT patch bonded on it. The related interaction model is shown in Fig. 1 for a square PZT patch of length 2¬ and thickness h.

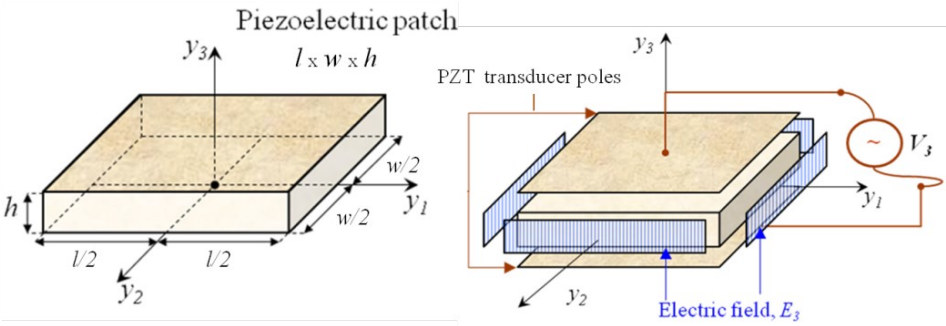

Figure 1: Interaction model of PZT and concrete structure.

Let's say that a sinusoidal voltage signal is generated across PZT electrodes. This signal can be expressed as a function of time in the form:

$$V_{pzt}(t)=V_p\sin(\omega t) \qquad (1)$$

where V_{pzt} (t) is the voltage across the direction of the axis y_3 at time t, V_p is the peak voltage of the voltage signal and ω is the radial frequency. The relationship between radial frequency ω (in radians/second) and frequency f (Hz) is $\omega=2\pi f$.

In a linear system, the response current signal I(t) is shifted in phase φ and has a different peak current I_p:

$$I(t)=I_p\sin(\omega t+\varphi) \qquad (2)$$

Taking into account that every PZT under a pure and high frequency sinusoidal voltage signal behaves almost like a capacitive system which tends to preserve negligible phase difference between voltage and current output signal, the impedance amplitude can be evaluated by

$$|Z(\omega)|=\frac{V_p(\omega)}{I_p(\omega)}\cong\frac{V_p(\omega)}{\frac{V_¿(\omega)}{|Z(\omega)|+R_f}} \qquad (3)$$

Then, the peak value $V_p(\omega)$ of the voltage V_{pzt} across the PZT transducer is estimated by solving the previous equation in terms of Vp(ω):

$$V_p(\omega) \cong \frac{|Z(\omega)|}{|Z(\omega)| + R_f} \cdot V_i \quad (4)$$

Based on the above equation, it is obvious that $V_{pzt}(\omega)$ and particularly the peak voltage signal $V_p(\omega)$ provides a solid indication for the value of |Z| being directly dependent on any observed impedance amplitude variations.

In the present work, an innovative structural monitoring system denoted as WiAMS proposed by the present authors in [7, 8] is further investigated to detect damage in concrete structures. WiAMS is a wireless system for estimating the impedance magnitude |Z| of a PZT device that is utilized for concrete integrity monitoring. Particularly, WiAMS offers extensive features such as remote control, high processing power, wireless data upload to SQL database, email notifications, scheduled, iterative |Z| estimations and frequency span from 5 kHz to 300 kHz resolution down to 1 Hz. WiAMS is consisted of multiple custom-made modules that conduct the |Z| estimation and the architecture is depicted in Fig. 3. Particularly the modules are:

1. A single board computer (SBC) Raspberry Pi.
2. A custom board with the AD7357 ADC.
3. A custom board with the AD9837 frequency generator.
4. A custom interface board responsible for the power supply and the connection of the rest modules between them and with the Raspberry Pi.
5. The PZT driver module.

The core hardware element of WiAMS which has been used as SBC in this work is the second version of Raspberry PI also known as Raspberry Pi model B as shown in Figure 2. Raspberry PI is the central control unit of WiAMS because it communicates and controls the integrated circuit modules of the system. Also due to its connection to the Internet, enables the user to control the system remotely using a terminal emulator (in the present work, PUTTY free open source application), be informed via mail and sends itself Raspberry pi measurement results for storing reasons to web databases. Due to its small size and weight (Raspberry Pi is credit card-sized) it can be placed on the specimen under test without affecting its dynamic features. Additionally, considering the device's low cost, a number of devices can be used for simultaneous scanning of a large scale structure.

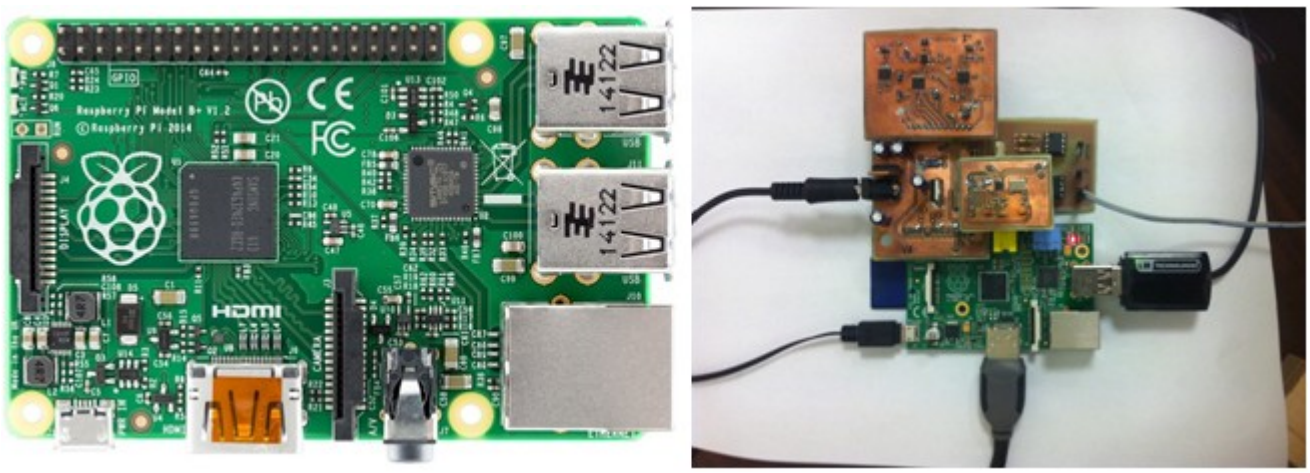

Figure 2: Raspberry Pi SBC (left), WiAMS Prototype (right)

3. DAMAGE INDEX BASED ON ELLIPTICAL AND CIRCLULAR MEASURE OF ERRORS

Let assume that the peak output voltage response signal measurements for the healthy baseline structural condition at any predefined frequency range ω_i (i=1,..No) is denoted by X_h while for any other different from healthy baseline structural condition, the peak output voltage response signal measurements at the same frequencies is denoted by Y_d. Let also assume that the pair X_h and Y_d may be considered as random normal, or Gaussian, variables which can be expressed in vector form as [11-12]:

$$Z=\begin{bmatrix} X \\ Y \end{bmatrix} \tag{5}$$

The mean of this Gaussian random vector is defined as

$$E[Z]=E\begin{bmatrix} X \\ Y \end{bmatrix}=\begin{bmatrix} m_X \\ m_Y \end{bmatrix} \tag{6}$$

The covariance matrix of the error vector is written as

$$\Sigma=\begin{bmatrix} \sigma_X^2 & \sigma_{XY} \\ \sigma_{XY} & \sigma_Y^2 \end{bmatrix} \tag{7}$$

Where σ_X^2 and σ_Y^2 are the variances of the random variables X_h and Y_d and σ_{XY} is the covariance of X_h and Y_d. The correlation coefficient of the variables X and Y is defined as

$$\rho=\frac{\sigma_{XY}}{\sigma_X \sigma_Y} \tag{8}$$

According to the previous definitions, the covariance matrix can be rewritten as

$$\Sigma=\begin{bmatrix} \sigma_X^2 & \rho\sigma_X\sigma_Y \\ \rho\sigma_X\sigma_Y & \sigma_Y^2 \end{bmatrix} \tag{9}$$

For this second-order case, the Gaussian PDF is defined as

$$f(z)=\frac{1}{2\pi\sqrt{det\,\Sigma}}\exp\left[\frac{-1}{2}\left[x-m_X\cdot y-m_Y\right]\Sigma^{-1}\left[x-m_X\cdot y-m_Y\right]^T\right] \tag{10}$$

$$¿\frac{1}{2\pi\sigma_X\sigma_Y\sqrt{1-\rho^2}}\exp\left[\frac{-1}{2(1-\rho^2)}\left(\frac{(x-m_X)^2}{\sigma_X^2}-\frac{2\rho(x-m_X)(y-m_Y)}{\sigma_X\sigma_Y}+\frac{(y-m_Y)^2}{\sigma_Y^2}\right)\right]$$

The locus (X_h,Y_d) for which the PDF is greater or equal to a specified constant K1 is given by

$$\left\{(x,y):\frac{1}{2\pi\sqrt{det\,\Sigma}}\exp\left[\frac{-1}{2}\left[x-m_X\cdot y-m_Y\right]\Sigma^{-1}\left[x-m_X\cdot y-m_Y\right]^T\right]\geq K_1\right\} \tag{11}$$

Equation (11) represent all the pairs (x_h,y_d) for which the PDF is less or equal to a given specified constant K_1. The locus of constant value is an ellipse with the axis parallel to the X_h, Y_d coordinates when $\rho=0$, i.e. when the random variables X_h and Y_d are uncorrelated (Figure 3a). When $\rho\neq0$ the ellipse axis are not parallel with the x_h and y_d axis. The center of the ellipse coincides in all cases with (m_X, m_Y). The locus in Eq.7 is the border and the inner points of an ellipse, centered in (m_X, m_Y). The length of the ellipses axis and the angle they do with the axis x_h and y_d are a function of the constant K, of the eigenvalues λ_1 and λ_2 of the covariance matrix Σ and of the correlation coefficient.

With no loss of generality, in the case of $m_X=m_Y=0$, i.e., the ellipse is centered in the coordinated frame, the coordinate system (x_h,y_d) is transformed to a new coordinate system axis w_1, w_2 which is rotated around the origin by an angle evaluated as

$$a=\frac{1}{2}\tan^{-1}\left(\frac{2\rho\sigma_X\sigma_Y}{\sigma_X^2-\sigma_Y^2}\right),-\frac{\pi}{4}\leq a\leq\frac{\pi}{4},\sigma_X\neq\sigma_Y \tag{12}$$

This ellipse is denoted as confidence ellipse. In the special situation of equal eigenvalues, i.e, $\lambda_1=\lambda_2$ we

have the case of confidence circle. If we denote the ratio of σ_Y/σ_X as the ellipticity parameter c then when c is equal to 1 the confidence ellipse becomes the confidence circle of the same probability while when c=0 the confidence ellipse degenarates into a line (linear degeneracy). Taking this into account, we introduce a new damage index based on the ratio between the area of the confidence ellipse generated for a specific confidence level, i.e., let's say 99.5%, and the area of the confidence circle with the same confidence level. This new damage index, denoted here as ECAR (Ellipse-to-Circle-Area-Ratio) index has the following form:

$$ECAR = \frac{Area\,of\,a\,confidence\,ellipse\,of\,a\,given\,probability}{Area\,of\,the\,confidence\,^{\circ}for\,the\,same\,probability \wedge confidence\,level}$$

ECAR index has the benefit that could directly characterize the degree of divergence existed between the healthy baseline and any current structural integrity condition since the divergence between the area of confidence ellipse of interest and the confidence circle of equivalent probability increases as the ellipse becomes thinner and more elongated, which is exactly the case where current structural integrity condition is very close to the healthy one, which, equivalently in turn, could be considered as an indicator of no damage case.

4. DESCRIPTION OF EXPERIMENTAL SETUP AND PROCEDURE

Experiments are conducted by mounting three PZT patches embedded in a different 100X150X750 mm concrete beam specimen, i.e., Specimen C1, in a setup shown in Figure 3. The concrete beam specimens were made by a mixing proportion of 1:0.62:2.25:3.83 (Cement: Water: Fine Aggregate: Coarse Aggregate, ratio by mean of cement). The investigated beam specimen was reinforced with one rebar of structural steel (10mm diameter, B500C class) in order to ensure shear failure with minimum restriction of the bending crack in the middle of the specimen. Three PZT actuator/sensors were bonded on the specimen surface taking into account that two of the PZT transducers (SD1 and SD2) serve as shear failure sensors while the third PZT transducer serve as bending crack sensor.

The baseline measurements were taken after placing the beam to its final position on the bending machine. Three measurements were taken in the unloaded state and their average was used as the baseline measurement of the pristine state. Afterwards, the concrete specimen was subjected to three point bending loads until failure. Measurements were taken at the end of each loading level as different damage stages exist in the structure. The first load level was for very low force in order to ensure that the tensile strength of the concrete is not exceeded and there are no cracks present yet (f_{ct} expected to be exceeded for a load of about 8 to 10 kN).

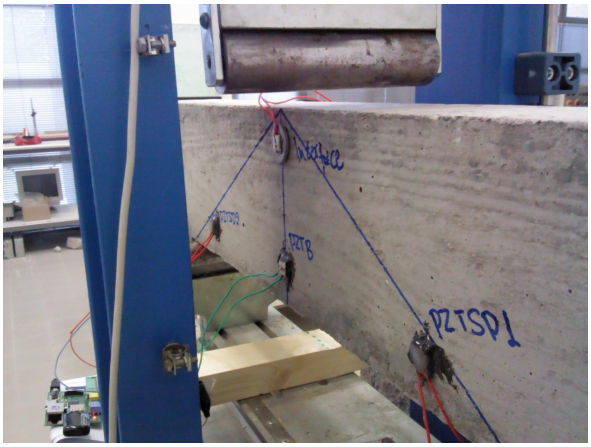

Figure 3: Three point bending loading experimental setup and PZT locations

The sequential load levels for specimen C1 are shown in the table below:

Load Case	Load 1	Load 2	Load 3	Load 4	Load 5	Load 6	Load 7	Load 8

Force (kN)	7.28	17.72	25.14	30.08	35.55	40.43	41.79	manual
PZT-B crack	no	YES	yes	yes	yes	yes	yes	yes
PZT-SD1 crack	no	no	no	no	YES	yes	yes	yes
PZT-SD2 crack	no	no	no	no	no	No	no	no

The last load case was taken after the complete failure of the beam and was manually controlled in order to widen the existing cracks. The frequency plots as well as the plots of the damage index introduced in this paper are shown in the following pages. It is worth mentioning that the bending crack appeared in the second load case (Load=17.72 kN) with the crack path passing directly through PZT-B (Figure 3) explaining the great difference in the frequency plots as well as the damage index. The beam was expected to fail due to shear force which is actually the case. The failure as expected occurred shortly after the appearance of the first shear crack, without the appearance of second shear crack as it was very lightly reinforced. The crack firstly appeared in load case 5 (Load=35.5 kN) and then was propagated up to failure in load case 8 as shown in Figure 4.

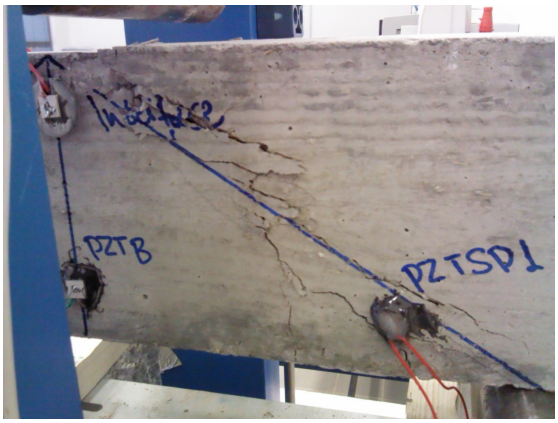

Figure 4: Path of shear crack in the vicinity of PZT-SD1 (Load Case 8)

The frequency plots shown in Figure 5 represent the spectrums of the detected voltage amplitude (in mV) versus frequency at the electrodes of PZT-B and PZT-SD1, respectively, transducers. The depicted results are the voltage across the PZT patch in the frequency domain, sweeping a specific range of frequencies specified by the user. In our case the sweeping range was 50-250 kHz with a frequency increment of 1 kHz. For frequencies lower than 50 kHz changes in the structural integrity of the structure will be "drowned" by the capacitive nature of the PZT in that specific bandwidth, and for frequencies higher than 250 kHz the PZT patch is more sensitive in changes of its own conditions rather than changes in the structure. Therefore, changes in the peak output voltage measured across the PZT electrodes result in changes between the pristine state and the damaged state which will be used as alarm for damage detection. As far as ECAR (Ellipse-to-Circle-Area-Ratio) damage index is concerned, figures 6 and 7 are the visual outcomes of what is described in previous chapter 3. The axes shown in those figures are peak output voltage for the baseline state vs. peak output voltage for any current loading state and what is graphically shown are the confidence ellipse and the confidence circle for a confidence level of 99.5%. The images are for baseline measurement and load case 1 (left image, low damage i.e. ellipse degenerates to line) and baseline measurement and load case 8 (right image, damaged state). The ratio of the area of the ellipsoid to the area of the circle is used as the ECAR damage index (figure 8).

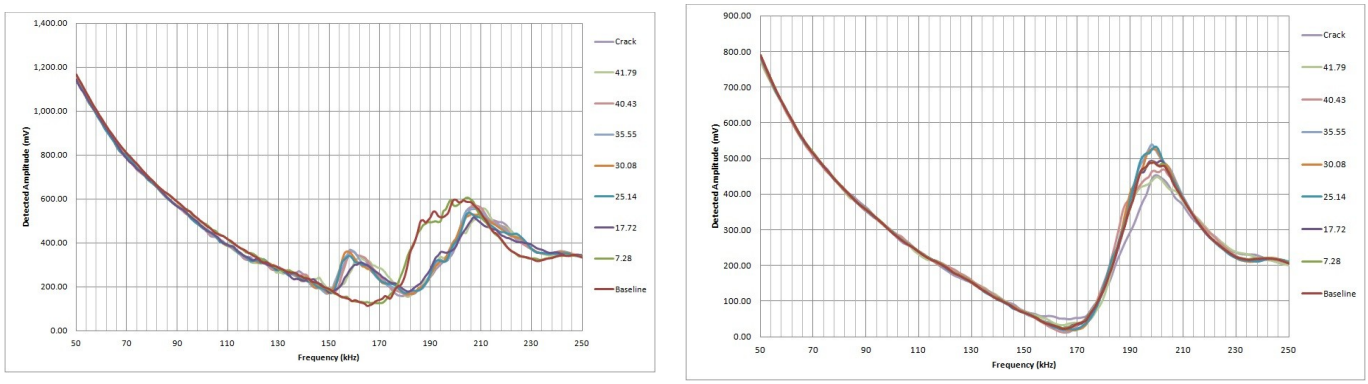

Figure 5: Peak Voltage Output spectrum plot for PZT-B and PZT-SD1 transducers

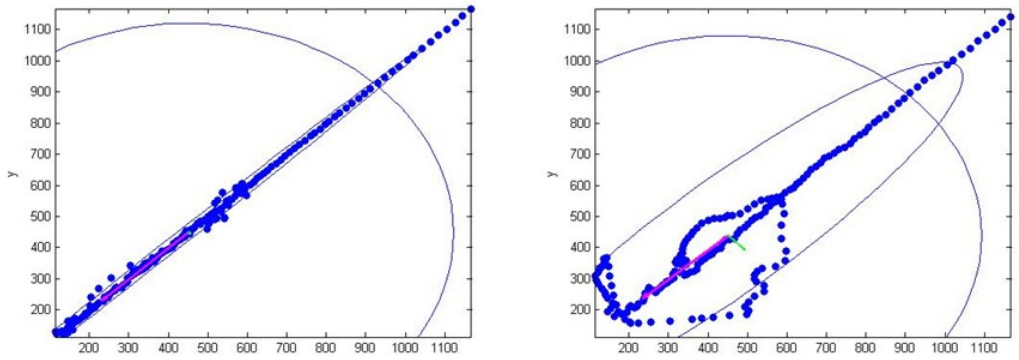

Figure 6: Plots of confidence ellipse-circle of the damage index for Load 1 (Left) and Load 8 (Right) (PZT-B)

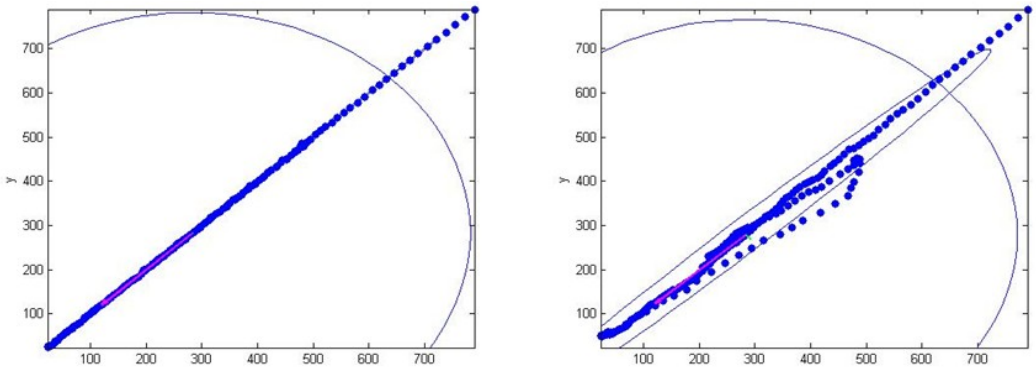

Figure 7: Plots of confidence ellipse-circle of the damage index for Load 1 (Left) and Load 8 (Right) (PZT-SD1)

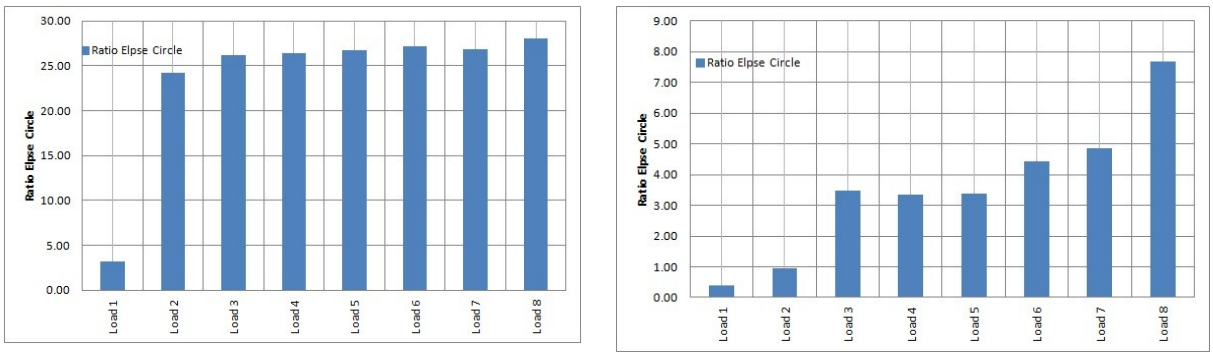

Figure 8: ECAR Damage index for PZT-B and PZT-SD1

5. CONCLUSIONS

This paper presents an innovative wireless structural health monitoring system based on an alternative version of electromechanical impedance (admittance) technique. The feasibility of the proposed WiAMS has been investigated by using a new damage identification index based on the implementation of statistical confidence regions as being the confidence ellipse and the confidence circle under specific confidence level. The WiAMS was successfully applied to laboratory experiments on concrete beam specimens. The proposed monitoring system was able to successfully correlate peak output voltage response signals to the onset of damage while in the same time its performance depends on the specific characteristics of its components. The results demonstrated that WiAMS gives the benefit of damage detection in early stages of concrete structures.

Acknowledgements: This research has been co-financed by the European Union (European Social Fund-ESF) and Greek National Funds through the Operational Programme "Education and Lifelong Learning" of the National Strategic Reference Framework (NSRF 2007-2013) of the Ministry of Education & Religious Affairs, Culture & Sports - Research Programme: THALES. The authors would also like to acknowledge the valuable suggestions of Professor Pol Spanos, Rice University, USA which have made the present research to be successfully performed.

REFERENCES

[1] Park G., Cudney H.H., and Inman D.J., Impedance-based health monitoring of civil structural components. *InfrastucturesSystems* 6, 153-160.2,2000.

[2] Park G., Cudney H.H. and Inman D.J., Overview of piezoelectric impedance-based health monitoring and pth forward.*The Shock and Vibration Digest* 35, 451-463.3, 2000.

[3] Song G., Gu H., Mo Y.L., Hsu T. and Dhonde H., Concrete structural health monitoring using embedded piezoceramic transducers, *Smart Mater. Struct.,* 16, 959-968, 2007.

[4] Giurgiutiu V., Zagrai A., Bao J.J., Damage identification in aging arcraft structures with piezoelectric wafer active sensors.*Journal of Intelligent Materialsm Systems and Strucures*.

[5] Cuc A., Giurgiutiu V., Disbond detection in adhesively-bonded structures using piezoelecetric wafer active sensors, Proceedings of SPIE *The International Society of Optical Engineering*, 5394, 66-77, 2004.

[6] Wai J.R., Park G., Farrar C.R., Integrated structural health monitoring assessment using piezoelectric active sensors. *Shock and Vibration*, 12(6), 389-405, 2005.

[7] Providakis C.P., Tsistrakis S., Voutetaki M., Tsompanakis J, Stavroulaki M., Agadakos J., Kampianakis E. and Pentes G., WiAMS: An innovative wireless damage detection monitoring system using electromechanical impedance-based and extreme value statistical approach, *Journal of Structural Control and Health Monitoring*, submitted, 2015.

[8] Providakis C.P., Stefanaki K.D., Voutetaki M., Tsompanakis J., Stavroulaki M., Damage detection in concrete structures using simultaneously activated multi-mode PZT sensing system. *Structure and Infrastructure Engineering*, 2013, DOI: 10.1080/15732479.2013.831908.

[9] Soh C.K. and Bhalla S., Structural Health Monitoring by Piezo-impedance Transducers I: modeling.*Journal of Aerospace Engineering*, ASCE 17, 154-165, 2004.

[10] Zhou S.W., Liang C.A., Rogers C.A., Integration and Design of Piezoceramic Elements in Intelligent Structures. *Journal of Intelligent Materials Systems and Structures* 6, 733-743,1995.

[11] Mertikas S., Error distributions and accuracy measures in navigation: an overview. Technical Report, February 1985, University of New Brunswick, Canada.

[12] Chin G.Y., Two dimensional measures of accuracy in navigational systems. Technical Report DOT-TSC-RSPA-87-1, 1987. US Dept of Transportation.